




Microstructure and mechanical properties of a novel hot-rolled 4% Mn steel processed by intercritical annealing

He-song Wang¹, Guo Yuan^{1,*} , Meng-fei Lan¹, Jian Kang¹, Yuan-xiang Zhang¹, Guang-ming Cao¹, R. D. K. Misra², and Guo-dong Wang¹

¹State Key Laboratory of Rolling and Automation (RAL), Northeastern University, Shenyang 110819, China

²Laboratory for Excellence in Advanced Steel Research, Department of Metallurgical, Materials and Biomedical Engineering, University of Texas at El Paso, El Paso, TX 79968, USA

Received: 30 January 2018

Accepted: 26 May 2018

Published online:

4 June 2018

© Springer Science+Business Media, LLC, part of Springer Nature 2018

ABSTRACT

The study described here focuses on the microstructure and mechanical properties of a novel hot-rolled medium-Mn steel (Fe–0.25C–4Mn–1.88Al–0.6Si–0.04Nb–0.08V, wt%) that contained only 4 wt% Mn and modest Al content of 1.88 wt%. It was found that a relatively high content (25–53 vol%) of retained austenite was obtained by intercritical annealing process. With increase in intercritical annealing temperature from 700 to 740 and to 760 °C, retained austenite fraction increased from 25.1 to 53.2% and then decreased to 46.1%. Besides, mechanical stability of retained austenite in 700–760 °C intercritically annealed steels decreased with increase in intercritical annealing temperature. The 720 °C intercritically annealed steel yielded excellent mechanical properties with yield strength of 766 MPa, tensile strength of 951 MPa, total elongation of 48.6% and PSE of 46.22 GPa·%, achieved by a high volume fraction of retained austenite (46%) with relatively high mechanical stability. Thus, the 4% Mn steel present in this study indicated excellent mechanical properties of medium-Mn steels can be achieved using low alloy content.

Introduction

In recent years, the third-generation advanced high strength steels have attracted significant interest because of outstanding combination of strength and ductility. Medium-Mn steels (4–10 wt% Mn content) are considered to be one of the most promising third-generation advanced high strength steels [1].

Medium-Mn steels have an ultrafine-grained microstructure resulting from the heat treatment in austenite + ferrite two phase region (intercritical annealing) [2, 3]. High content (20–60 vol%) of austenite can be obtained in medium-Mn steels, which has significant influence on mechanical properties [4–7].

Address correspondence to E-mail: yuanguoral@163.com

In typical Fe–Mn–C medium-Mn steels, a relatively long holding time in the intercritical temperature region is required to develop austenite-ferrite duplex structure [8, 9]. This is because Mn decreases the intercritical annealing temperature, which decreases the kinetics of austenite formation. For example, Shi et al. [10] reported that a Fe–0.2/0.4C–5/7Mn (wt%) steel exhibited tensile strength of 1–1.5 GPa and ductility of 31–44%, which required intercritical annealing time of 6 h at 650 °C. Adding relatively high content of Al to medium-Mn steels can enhance A_{e1} and A_{e3} temperature, such that intercritical annealing has to be performed at higher temperature, which contributes to the decrease in intercritical annealing time [11]. Besides, high content of Al added to medium-Mn steels was beneficial in obtaining a desirable fraction of austenite by suppressing excessive transformation of intercritical austenite and enhancing C and Mn partitioned into intercritical austenite [11]. Thus, medium-Mn steels alloyed by high content of Al have been developed and outstanding mechanical properties are obtained. For examples, Li et al. [12] reported that PSE (product of tensile strength and total elongation) of 43.7 GPa% was obtained in a hot-rolled Fe–0.2C–8.5Mn–3Al (wt%) steel after annealing at 750 °C for 1 h. Cai et al. designed a cold-rolled Fe–0.18C–11Mn–3.8Al (wt%) steel, which exhibited PSE up to 65 GPa% after annealing at 770 °C [13]. Although excellent mechanical properties have been obtained in these recently developed Mn–Al medium-Mn steels, they are not cost effective and there are difficulties in processing steel with high Mn and Al content [3]. High Mn content in medium-Mn steel requires more heat input to melt ferromanganese alloys. Additionally, the high Mn content in medium-Mn steel leads to Mn segregation during solidification and decreases thermal conductivity of continuous casting slabs. This may cause internal cracks between columnar grains in slabs because of large thermal stress gradient during cooling [3]. Thus, it is important to fundamentally understand and explore mechanical behavior of medium-Mn steel with low Mn and Al content.

Based on the prior literature, it can be summarized that previous works mainly focused on medium-Mn steels with Mn content of 5–10 wt% [7, 14–17]. The Al content in majority of Mn–Al medium-Mn steels was greater than 2 wt% [15]. Recently, the focus has been on medium-Mn steels with Mn content less than

5 wt%. Seo et al. [18] studied a Fe–0.2C–4.0Mn–1.6Si–1.0Cr (wt%) steel processed by quenching and partitioning (Q&P) process and cold-rolled 4 wt% Mn steels alloyed by Ti and Mo were studied by Lee et al. [7]. However, studies on hot-rolled medium-Mn steel with Mn content less than 5 wt% processed by intercritical annealing are rare. Austenite content, austenite stability and mechanical properties in hot-rolled medium-Mn steels with low alloy content are unclear. It is novel and interesting to study whether excellent tensile properties can be obtained in medium-Mn steel with low alloy content. In this study, we designed a novel hot-rolled medium-Mn steel (Fe–0.25C–4Mn–1.88Al–0.6Si–0.04Nb–0.08V, wt%) that contained only 4 wt% Mn and modest Al content of 1.88 wt%, but exhibited excellent tensile properties. Microstructure, mechanical properties and austenite stability in this hot-rolled 4% Mn steel processed by intercritical annealing were studied in detail.

Materials and methods

The chemical composition of the experimental steel is listed in Table 1. The fraction of equilibrium phase in the temperature range of 600–950 °C calculated by Thermo-Calc software combined with TCFE6 database is shown in Fig. 1. It can be seen that the start temperature and finish temperature of transformation from ferrite and Fe_3C to austenite were 640 and 700 °C, respectively.

A 90-kg ingot of the experimental steel was prepared by vacuum induction melting. The ingot was forged into a billet with a section dimension of 70 mm × 60 mm. The billet was homogenized at 1200 °C for 2 h and then hot-rolled to 4-mm-thick sheet involving nine passes. The finish rolling temperature was ~ 900 °C. After finish rolling, the sheet was finally cooled to room temperature in air. Subsequently, the as-hot-rolled sheet was subjected to intercritical annealing, which involved intercritical annealing at 700, 720, 740 and 760 °C for 60 min, respectively, followed by air cooling to room temperature. For convenience, the as-hot-rolled sheet

Table 1 Chemical composition of experimental steel (wt%)

C	Mn	Al	Si	Nb	V	Fe
0.25	4	1.88	0.6	0.04	0.08	Bal.

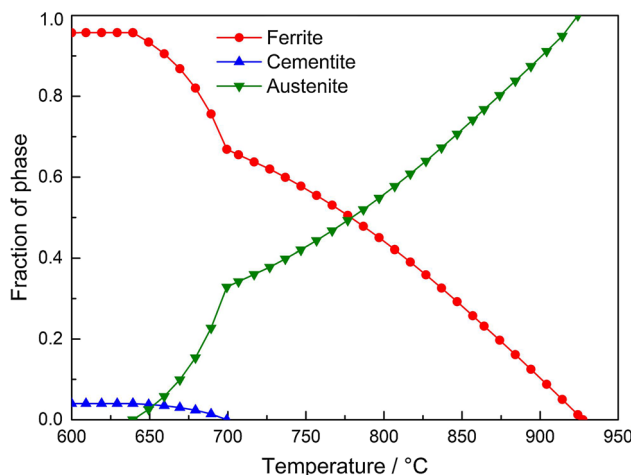


Figure 1 Fraction of equilibrium phases in the temperature range of 600–950 °C calculated by Thermo-Calc software combined with TCFe6 database.

intercritically annealed at 700, 720, 740 and 760 °C is referred to as A700, A720, A740 and A760, respectively.

Phase transformation temperature during heating and cooling was studied by a Formator-FII full-automatic thermal dilatometer. Cylindrical specimens (dimensions $\phi 3 \times 10$ mm) were used for dilatometry study. The microstructure of intercritically annealed sheets was observed by JXA-8530F electron probe microanalyzer (EPMA) after mechanical polishing and etching with 4% nital (time 30 s). Austenite phase and Schmid factor of austenite were determined by electron backscattered diffraction (EBSD) system attached to a Zeiss Ultra-55 field emission scanning electron microscope (SEM). Specimens for EBSD study were first mechanically polished and then electropolished (current ~ 0.8 A, time ~ 20 s) using an electrolyte consisting of perchloric acid and alcohol in the proportion of 1:7 at 22 °C. Microstructure, Mn content in different phases and chemical composition of precipitates were analyzed by Tecnai G² transmission electron microscope (TEM) equipped with energy-dispersive spectrometer (EDS) system. TEM specimen (diameter 3 mm) was first mechanically thinned to 50 μm and then twin-jet electropolished at -22 °C in a solution containing perchloric acid and alcohol in the proportion of 2:23.

The measurement of retained austenite (RA) content before and after tensile deformation (fractured sample) was taken by D/max2400 X-ray diffractometer (XRD) (Cu-K α radiation, scan rate 0.04°/s). Fractured samples tested by EBSD, TEM and XRD

were in the region that was ~ 6 mm away from the fracture surface. XRD sample was electropolished using a procedure identical to the EBSD sample. Integrated intensities of (200) α , (211) α , (200) γ , (220) γ and (311) γ diffraction peaks were selected for calculating the volume fraction of RA using Origin 8.6. The following equation was used to calculate the volume fraction of RA [19]:

$$V_{\gamma} = 1.4I_{\gamma} / (I_{\alpha} + 1.4I_{\gamma}) \quad (1)$$

where V_{γ} , I_{α} and I_{γ} are the volume fraction of RA, average integral intensities of ferrite and austenite peaks, respectively.

Tensile specimens of dimensions 6.25 mm (width) \times 4 mm (thickness) \times 25 mm (gauge length) were machined with longitudinal axis parallel to the hot rolling direction. The tensile test was performed using a universal testing machine (crosshead speed 2 mm/min, room temperature). The strain hardening rate (θ) was calculated using the following equation [20]:

$$\theta = d\sigma / d\varepsilon \quad (2)$$

where σ is true stress and ε is true strain.

Results

Dilatometer curves and microstructure

Figure 2 shows dilatometric curves of intercritically annealed specimens. The dilatometric specimens were heated to 700, 720, 740 and 760 °C at a heating rate of 5 °C/s and then were intercritically annealed

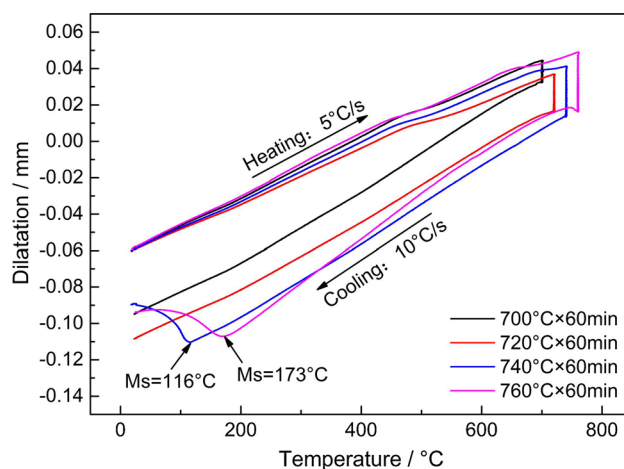


Figure 2 Dilatometric curves of specimens intercritically annealed at 700–760 °C for 60 min.

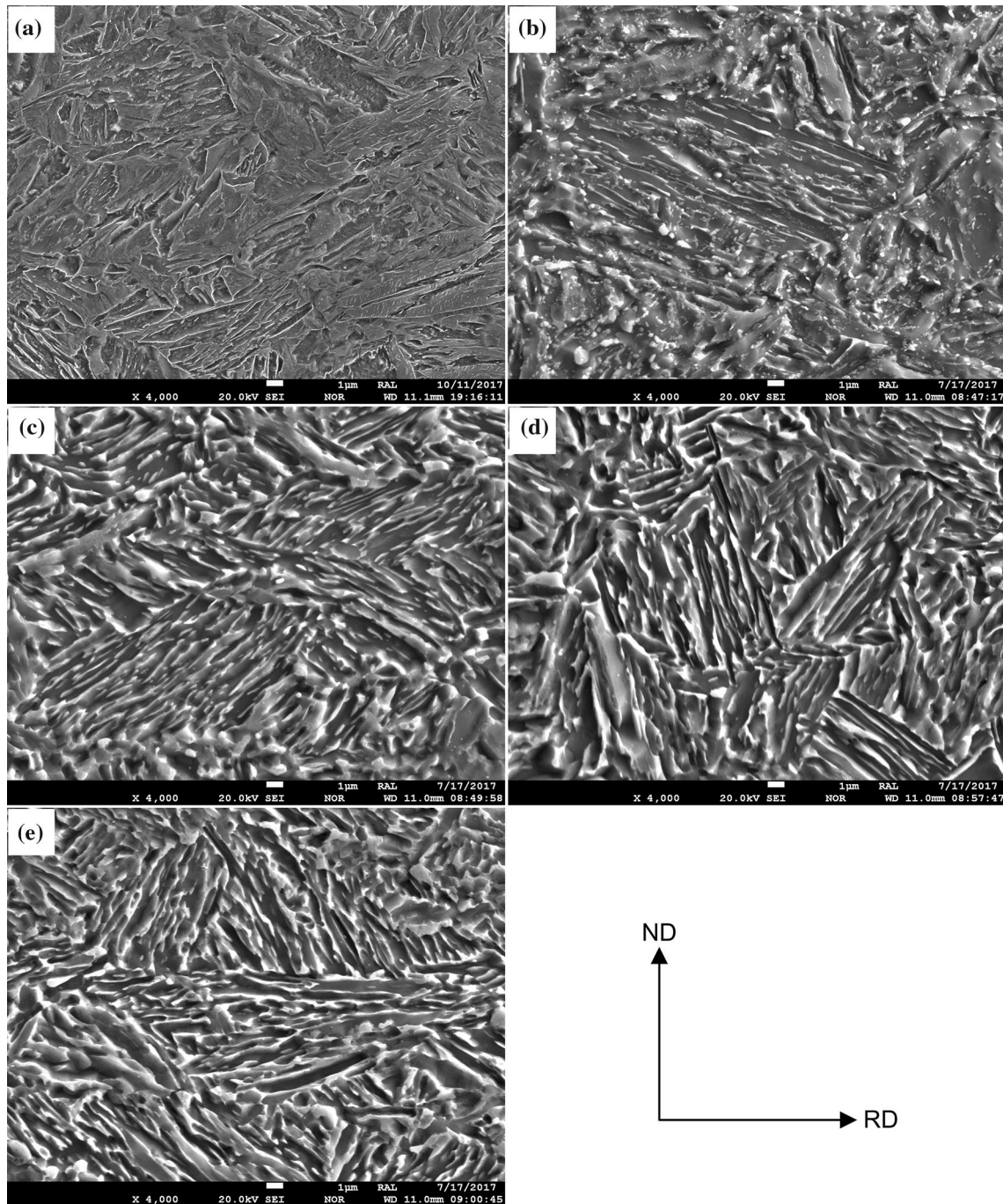


Figure 3 EPMA micrographs of **a** as-hot-rolled sheet, **b** A700, **c** A720, **d** A740 and **e** A760 steels. RD is rolling direction, and ND is normal direction.

for 60 min, followed by cooling to room temperature at a cooling rate of 10 °C/s. From Fig. 2, it was observed that no martensite transformation occurred in the sample intercritically annealed at 700–720 °C, while intercritical austenite formed during intercritical annealing at 740–760 °C transformed to martensite. The M_s temperature of 740 and 760 °C

intercritically annealed samples was 116 and 173 °C, respectively.

Figure 3 shows EPMA micrographs of as-hot-rolled sheet, A700, A720, A740 and A760 steels. In the as-hot-rolled sample, the microstructure consisted of martensite (Fig. 3a). When the intercritical annealing temperature was 700 °C, some of the martensite laths

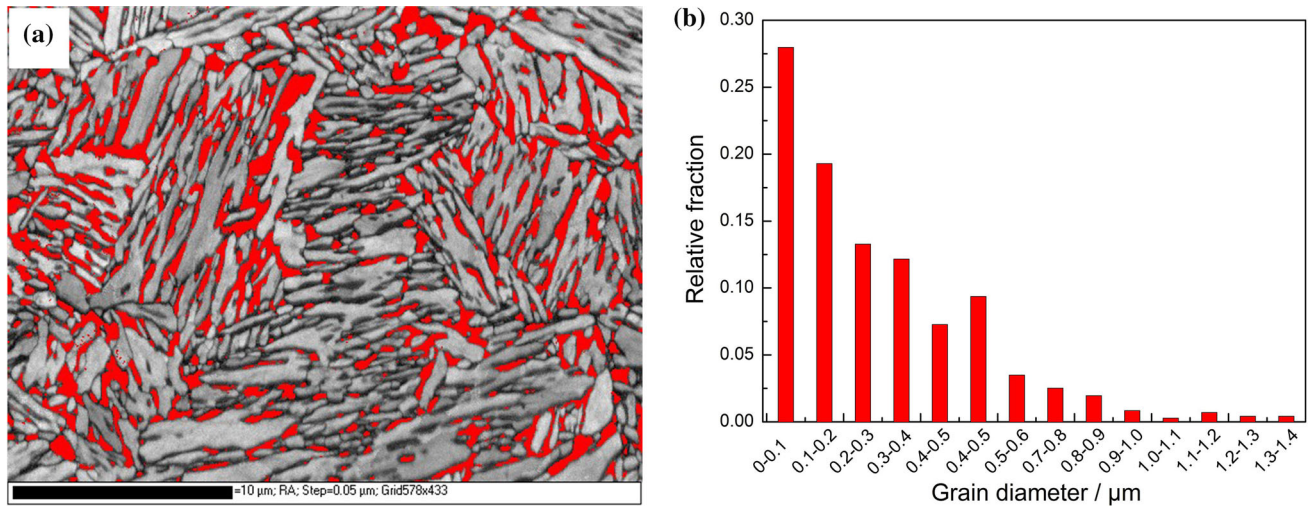


Figure 4 **a** EBSD micrograph of A720 steel and **b** distribution of RA grain size in A720 steel. The red part in **a** is RA. RA grain size was calculated using equivalent circled diameter.

were transformed into austenite laths, which were the hard-etched phases, i.e., the bright laths in Fig. 3b. At the same time, carbides were observed. With increase in intercritical annealing temperature to 720–760 °C, lamellar structure was more distinct (Fig. 3c–e). Based on the dilatometric curves (Fig. 2), it can be concluded that A720 steel possessed a duplex structure consisting of ferrite and RA. However, from the dilatometric curves (Fig. 2), there must be a small amount of martensite in A740 and A760 steels besides ferrite and RA. Additionally, in order to obtain the distribution of RA grain size in A720 steel, the microstructure of A720 steel was studied using EBSD and the result is shown in Fig. 4. The result confirmed that RA grain size was not uniform and was characterized by a wide distribution (Fig. 4b).

Figure 5 shows XRD patterns of undeformed and fractured samples, comparison of measured RA fraction and transformation ratio of RA between undeformed and fractured samples. Ferrite and austenite peaks were present in all the samples, while the austenite peaks of undeformed samples were of higher intensity than fractured samples (Fig. 5a and b). From Fig. 5c, it can be seen that with increase in intercritical annealing temperature from 700 to 740 °C, RA fraction was increased from 25.1 to 53.2%, while RA fraction was decreased from 53.2 to 46.1% on increasing the intercritical annealing temperature from 740 to 760 °C. RA fraction in fractured samples was decreased with the increase in annealing temperature. Besides, when the intercritical annealing

temperature was increased from 700 to 740 °C, the transformation ratio of RA in A700–A740 samples was obviously increased (Fig. 5d). The minimal transformation ratio of RA was 29.1% in A700 steel, while the maximal transformation ratio of RA was 93.8% in A740 steel.

Figure 6 shows TEM studies of undeformed sample of A720 steel. In Fig. 6a, lath-like RA and ferrite were observed. The corresponding EDS result of Mn distribution in RA and ferrite in Fig. 6a is shown in Fig. 6c. A total of 16 random points were selected, and the result showed that the average Mn content was 7.4 wt% in RA and 2.5 wt% in ferrite. This confirmed that Mn was enriched in austenite during intercritical annealing. Besides, it can be seen from Fig. 6b that precipitates with an average diameter of ~ 8–15 nm were observed in ferrite matrix, austenite matrix and the interface of ferrite and austenite. The EDS analysis indicated that the particle was (Nb, V)C (Fig. 6d) and VC (Fig. 6e).

Figure 7 shows TEM micrographs of fractured sample of A720 steel. The selected area electron diffraction (SAED) pattern (Fig. 7c) of the region identified by red circle in Fig. 7a indicated that it was a bcc crystal structure and the Mn content was 7.6 wt%, as determined by EDS in TEM. Thus, the red circle region was not ferrite, but martensite that transformed from RA during tensile deformation. Moreover, untransformed RA and stacking faults in RA were also observed in the fractured sample of A720 steel (Fig. 7d), as evidenced by dark-field image (Fig. 7e) and SAED pattern (Fig. 7f).

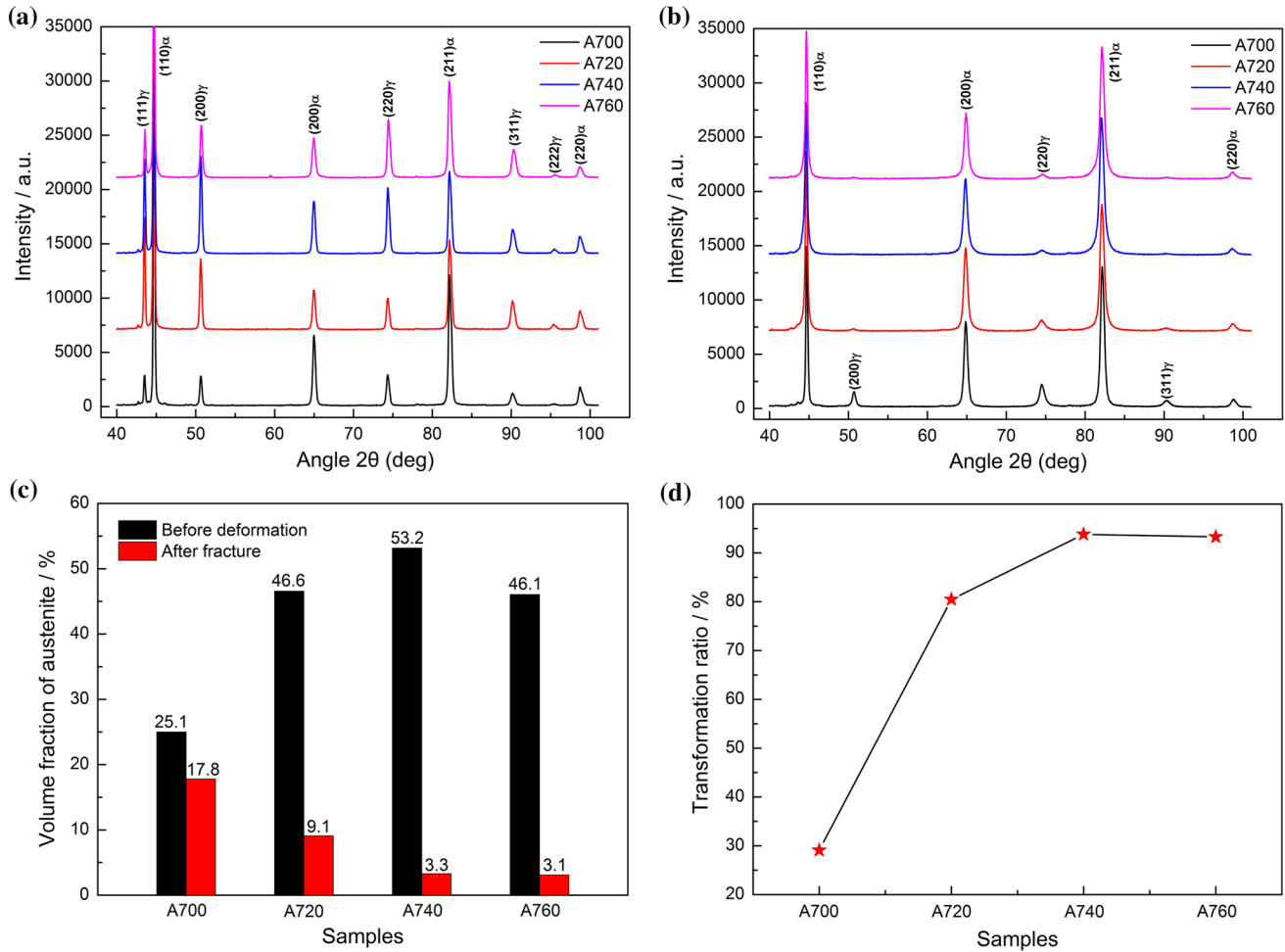


Figure 5 XRD patterns of **a** undeformed and **b** fractured samples, **c** comparison of measured RA fraction and **d** transformation ratio of RA between undeformed and fractured samples.

Figure 8 shows Schmid factor distribution map and corresponding statistical data of Schmid factor distribution of RA grain analyzed by EBSD. It can be seen from Fig. 8a, b that in A720 steel majority of RA grains had Schmid factor greater than 0.4 and the percentage was 93%. However, from Fig. 8c, d, it was observed that in the fractured sample of A720 steel, the percentage of RA grains with Schmid factor greater than 0.4 was only 30%.

Mechanical properties

Figure 9 shows room temperature engineering stress–strain plots of A700–A760 steels, and the corresponding mechanical properties extracted from the plots are listed in Table 2. It can be seen that mechanical properties were influenced by intercritical annealing temperature. As the intercritical

annealing temperature was increased, the tensile strength of intercritically annealed sheet was increased, while the yield strength was decreased. Yield ratio decreased with increase in intercritical annealing temperature, which implied a rapid increase in strain hardening. It should be noted that superior mechanical properties with yield strength of 766 MPa, tensile strength of 951 MPa and total elongation of 48.6% were obtained in A720 steel, leading to highest PSE of 46.22 GPa% in A720 steel. Moreover, the four engineering stress–strain curves were significantly different. Serrated fluctuation behavior was observed in A720, A740 and A760 steels, while no serrated fluctuation behavior was observed in A700 steel. Figure 10 shows work hardening rate–true strain curves of A700, A720, A740 and A760 steels. It can be seen that significant serrated fluctuation (multi-peak) was observed in the work

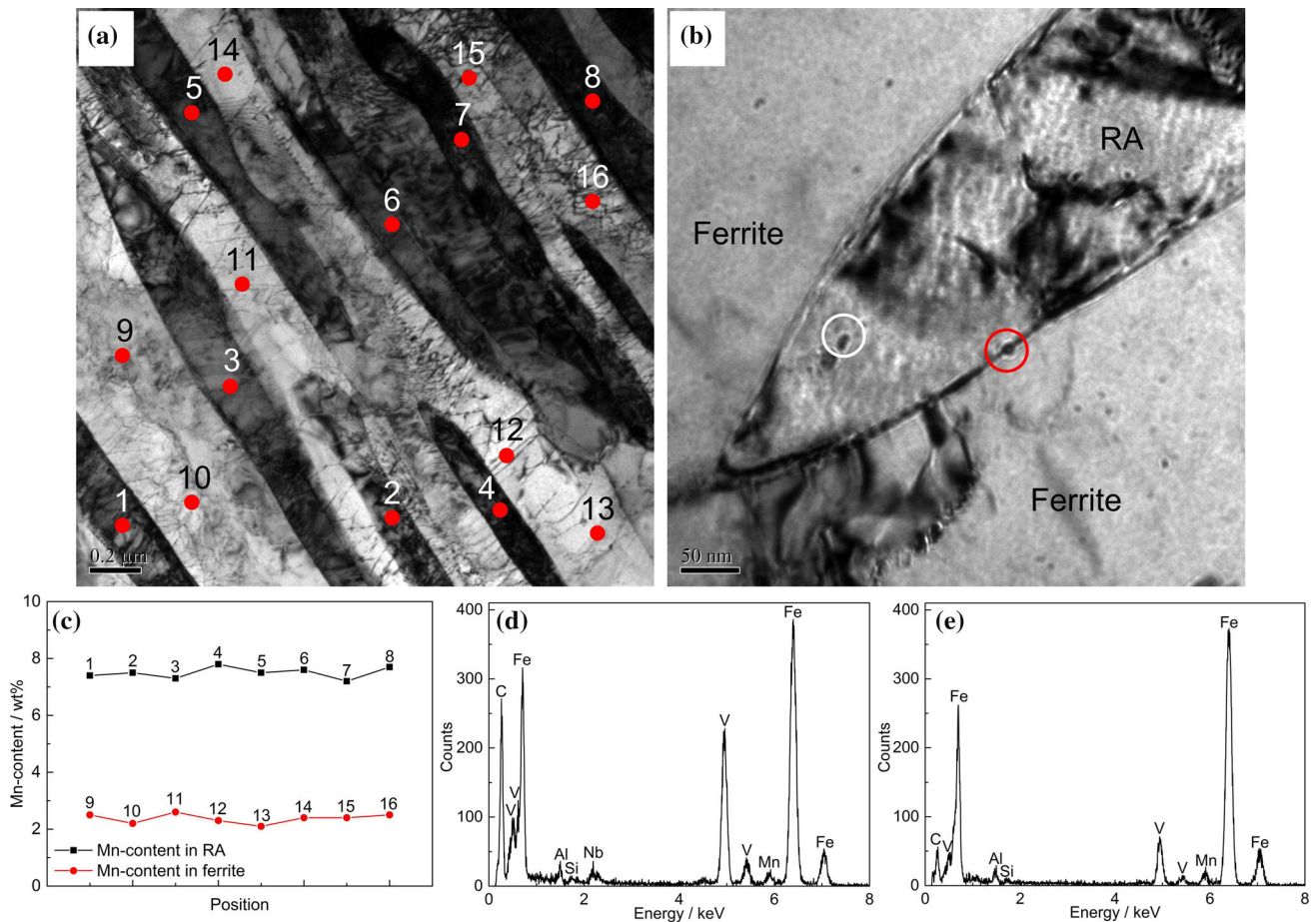


Figure 6 a, b TEM micrographs of undeformed sample of A720 steel, c corresponding Mn distribution in a by EDS and d, e EDS analysis of precipitate. EDS analysis of d and e was obtained from the precipitate denoted by white circle and red circle in b, respectively.

hardening rate–true strain curves of A720, A740 and A760 steels, consistent with the engineering stress–strain curves (Fig. 9).

Discussion

Thermal stability of intercritical austenite

With increase in intercritical annealing temperature from 700 to 740 and to 760 °C, RA fraction in A700–A760 steels was increased from 25 to 53%, followed by decrease to 46% (Fig. 5). Martensite transformation was observed in the dilatometer curves of A740–A760 steels, while no martensite transformation was observed in the dilatometer curves of A700–A720 steels. It can be inferred that thermal stability of intercritical austenite was significantly influenced by intercritical annealing temperature. Figure 11 shows the solute content of C, Si, Mn and Al in austenite in

the temperature range of 675–800 °C calculated using Thermo-Calc software combined with TCFE6 database. It can be seen that C and Mn contents in austenite obviously varied with temperature, while Al and Si contents were insensitive to temperature. Thus, intercritical annealing temperature influences the C and Mn contents in intercritical austenite. In the temperature range of 700–760 °C, C and Mn diffused to intercritical austenite during intercritical annealing process. However, with the increase in intercritical annealing temperature (700–760 °C), the intercritical austenite content was increased (Fig. 1), such that C and Mn contents in intercritical austenite were decreased (Fig. 11). C and Mn are strong austenite-stabilizing elements [21, 22]. Thus, thermal stability of intercritical austenite was decreased with the increase in intercritical annealing temperature. This led to martensite transformation present in 740–760 °C intercritically annealed steels. Besides, the decrease in RA fraction in A760 steel may be related

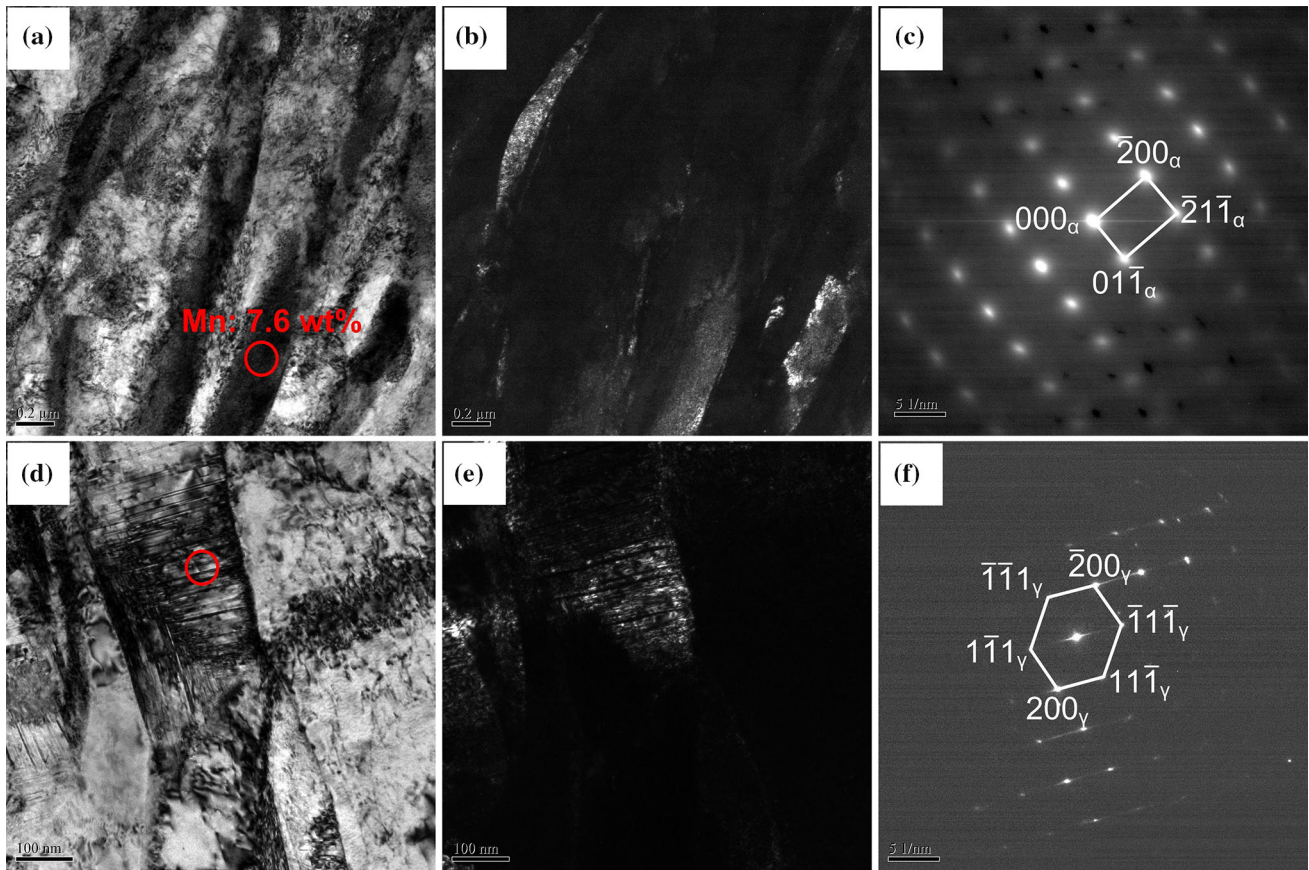


Figure 7 TEM micrographs of fractured sample of A720 steel: **a–c** bright-field image, dark-field image and corresponding SAED pattern of martensite transformed from RA and **d–f** bright-field

image, dark-field image and corresponding SAED pattern of untransformed RA. SAED patterns of **c** and **f** were obtained from the area denoted by red circle in **a** and **d**, respectively.

to the factor that thermal stability of intercritical austenite formed at 760 °C was relatively low, such that much intercritical austenite transformed to martensite. Moreover, it is well known that thermal stability of austenite decreases with the coarsening of austenite grains [23, 24]. In A740–A760 steels, the size of intercritical austenite formed during intercritical annealing may increase with increase in intercritical annealing temperature, which reduces thermal stability of intercritical austenite and contributes to martensite transformation.

Mechanical stability of RA

In medium-Mn steels, in order to have a better comparison of the mechanical stability of RA, the following equation was used [25]:

$$f_{\gamma\epsilon} = f_{\gamma 0} \exp(-k\epsilon) \tag{3}$$

where $f_{\gamma 0}$ is an initial value of the volume fraction of RA in the sample before tensile deformation and $f_{\gamma\epsilon}$ is

a value strained to fracture. The calculated k value of A700, A720, A740 and A760 steels was 1.7, 4.1, 10.6 and 12.7, respectively. A lower k value corresponds to higher mechanical stability of RA. It is apparent that the mechanical stability of RA in A700–A760 steels was decreased with increase in intercritical annealing temperature.

In this study, no serrated fluctuation was observed in the work hardening behavior in A700 steel, while serrated fluctuation was observed in the work hardening behavior in A720–A760 steels. Serrated fluctuation in the work hardening behavior in A720, A740 and A760 steels started at true strain of ~ 0.14 , ~ 0.025 and ~ 0.013 , respectively (Fig. 10). This may be related to mechanical stability of RA. RA with lower mechanical stability in A740 and A760 steels started transforming at a smaller strain and resulted in the premature appearance of serrated fluctuation in the work hardening behavior, which was similar to the observation in a hot-rolled Fe–0.2C–5Mn–1.5Al–

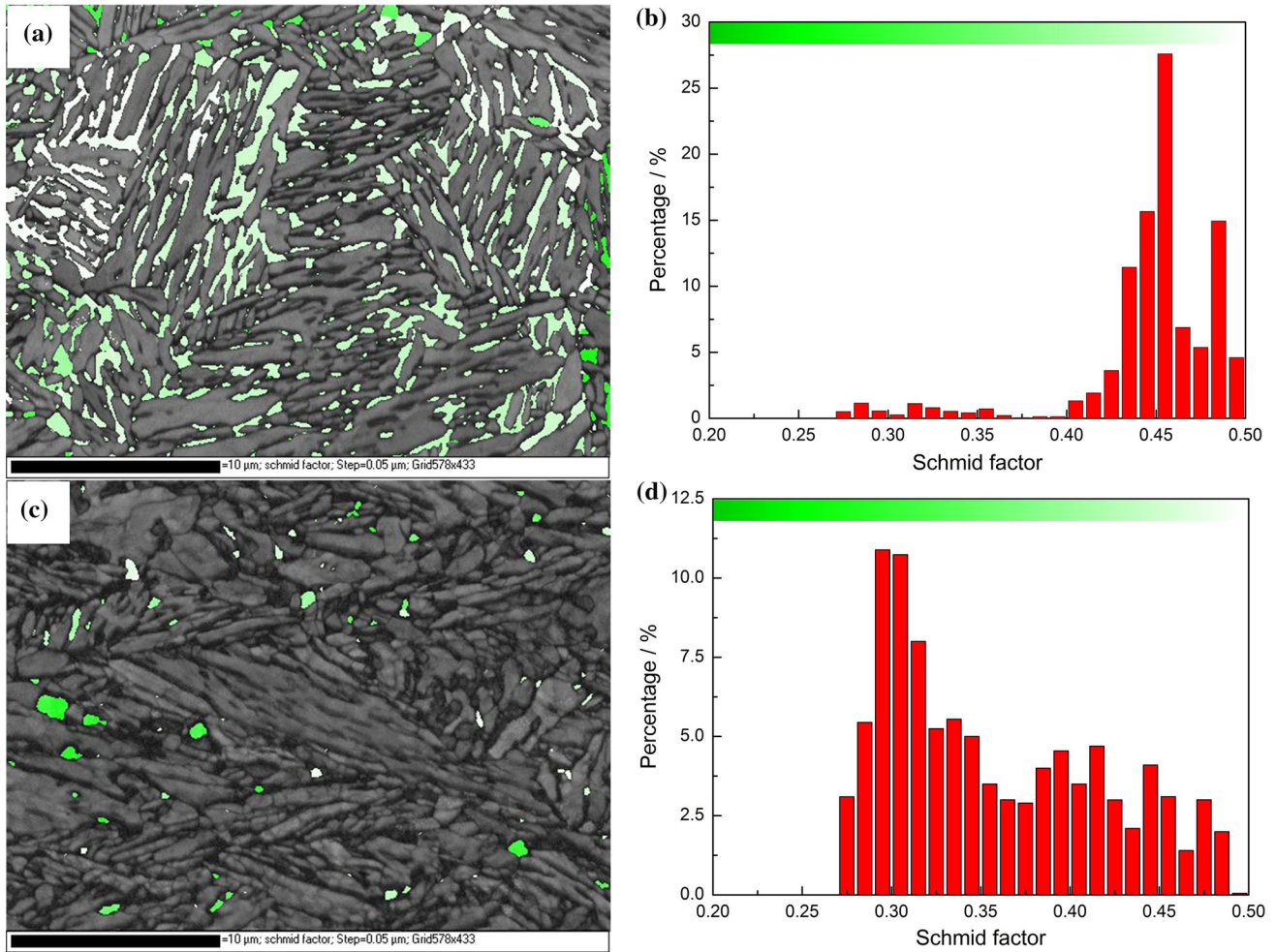


Figure 8 a, c Schmid factor distribution map and b, d corresponding statistical data of Schmid factor distribution of RA grain analyzed by EBSD: a, b undeformed sample and c, d fractured sample of A720 steel.

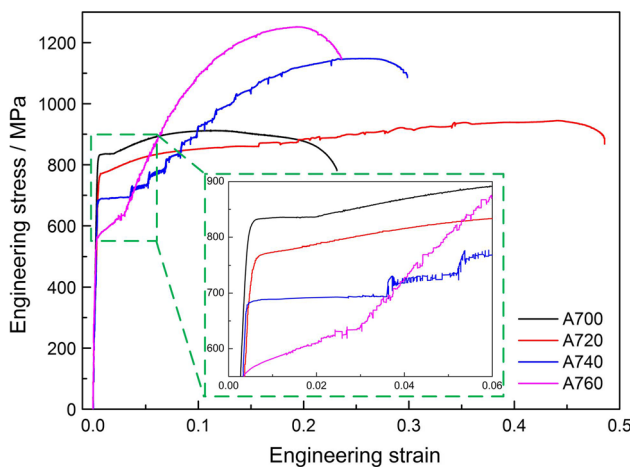
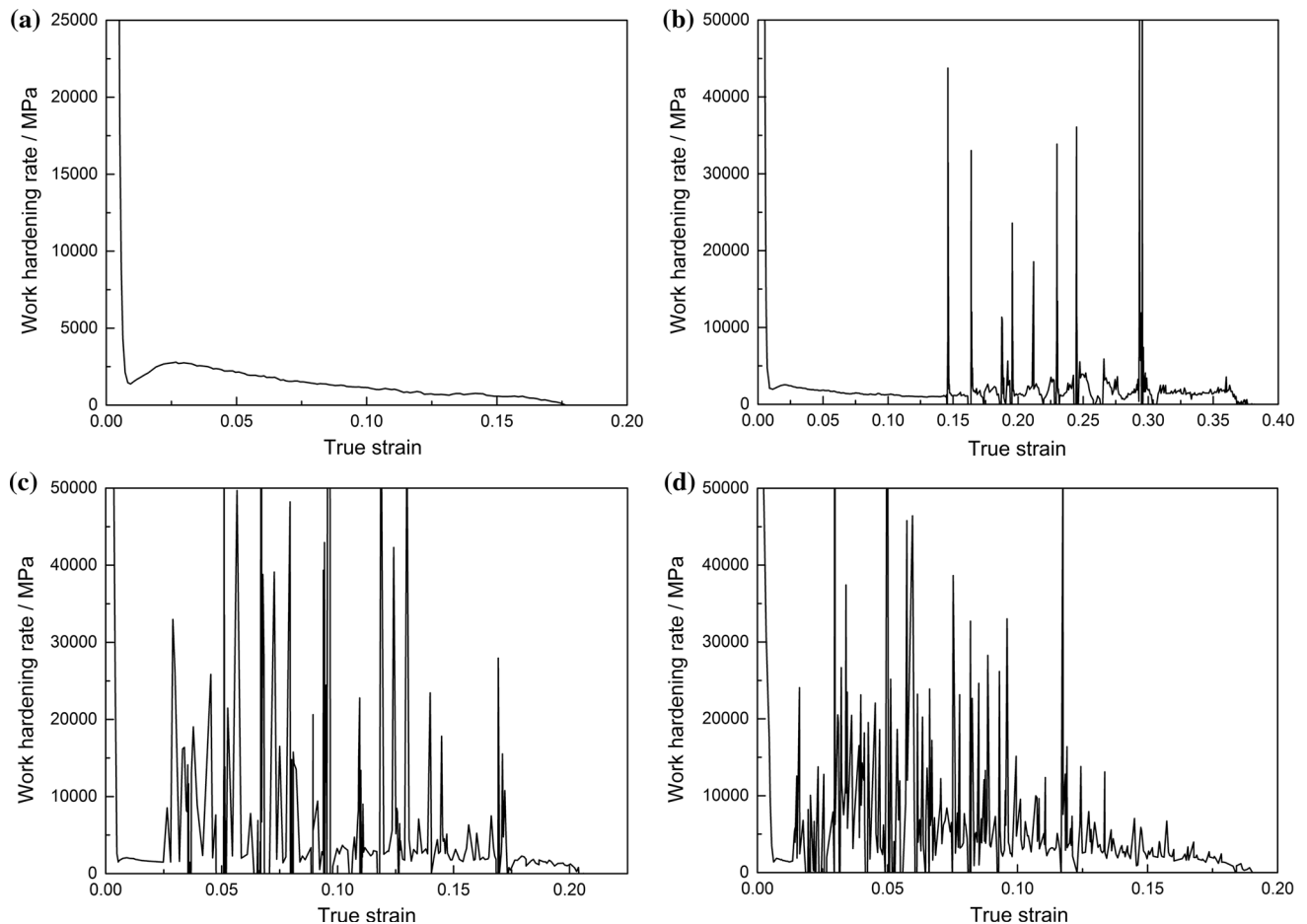


Figure 9 Room-temperature engineering stress–strain plots of A700–A760 steels.

0.5Si (wt%) steel [26]. Cai et al. [27] reported that the serrated fluctuation in the work hardening behavior of medium-Mn steels was related to discontinuous transformation induced plasticity (TRIP) effect involving stress relaxation and transfer during deformation with consequent enhancement in ductility. Besides, Xu et al. [26] also confirmed that the serrated fluctuation was attributed to the inhomogeneous and discontinuous occurrence of TRIP effect. Discontinuous TRIP effect primarily results from RA with different degree of mechanical stability [28, 29]. Thus, it is worth finding out the reason underlying the different degree of mechanical stability of RA. As for highest PSE obtained in A720 steel, we mainly focused on the factors resulting in inhomogeneous mechanical stability of RA in A720 steel. From the EDS result shown in Fig. 6c, we know that the Mn content in RA grains was similar and the average

Table 2 Mechanical properties of A700–A760 steels

Specimen	Yield strength/MPa	Tensile strength/MPa	Total elongation/%	PSE/GPa%	Yield ratio/%
A700	828	913	23.1	21.09	91
A720	766	951	48.6	46.22	81
A740	683	1143	29.9	34.18	60
A760	562	1251	23.6	29.52	45

**Figure 10** Work hardening rate-true strain curves of **a** A700, **b** A720, **c** A740 and **d** A760 steels.

content of Mn in RA was 7.4 wt%. As regards C content in RA, we consider that it was almost uniform in different RA grains because of its high diffusion coefficient. Thus, inhomogeneous mechanical stability of RA is not mainly related to Mn and C contents in RA grains. From the EBSD result shown in Fig. 4, RA grain size was not uniform and had a wide distribution. It is well known that mechanical stability of austenite is significantly influenced by grain size [28]. Mechanical stability of austenite decreases with increase in grain size, such that it can

be inferred that inhomogeneous mechanical stability of RA in A720 steel is related to the heterogeneity in RA grain size (Fig. 4). Besides, from the EBSD result shown in Fig. 4a, the morphology of RA was different. Both lath-like RA and blocky RA were observed. Previous studies confirmed that the mechanical stability of lath-like RA and blocky RA was different [18, 28]. Thus, it can be inferred that inhomogeneous mechanical stability of RA in A720 steel is also related to the morphology of RA. Moreover, the relative volume fraction of RA in A720 steel having the

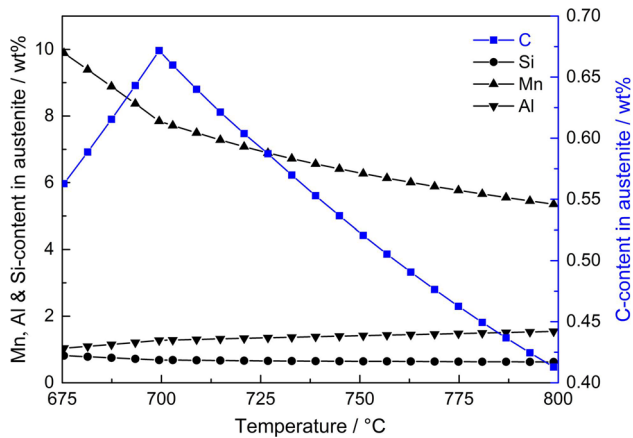


Figure 11 Solute content in austenite in the temperature range of 675–800 °C calculated by Thermo-Calc software combined with TCFE6 database.

Schmid factors smaller than 0.4 was $\sim 7\%$ before deformation and $\sim 70\%$ after tensile deformation (Fig. 8). The result indicated that the RA with small Schmid factor (< 0.4) in A720 steel tended to remain stable during tensile deformation. In a previous study, it was shown that when Schmid factor was less than 0.4, RA grain exhibited a considerable stability during deformation [30]. Thus, we believe that besides grain size and morphology of RA, inhomogeneous mechanical stability of RA in A720 steel is also related to Schmid factor of RA.

Mechanical properties

Figure 12 shows the variation of PSE, volume fraction of RA and k value in A700–A760 steels. It can be seen that the variation of PSE was not in accordance with the variation of volume fraction of RA. Highest volume fraction of RA was obtained in A740 steel, but highest PSE was not obtained in A740 steel. However, highest PSE of 46.22 GPa% was obtained in A720 steel. Thus, mechanical properties of A700–A760 steels was not only related to RA fraction, but also was related to the mechanical stability of RA.

From the k value shown in Fig. 12, it was known that mechanical stability of RA in A700 steel was relatively stable, which resulted in the relatively low transformation ratio of austenite to martensite (Fig. 5). Thus, TRIP effect cannot sufficiently occur in A700 steel, leading to a low PSE. However, in A720 steel, tensile strength and total elongation were higher than A700 steel. This is related to the result that both RA volume fraction and transformation

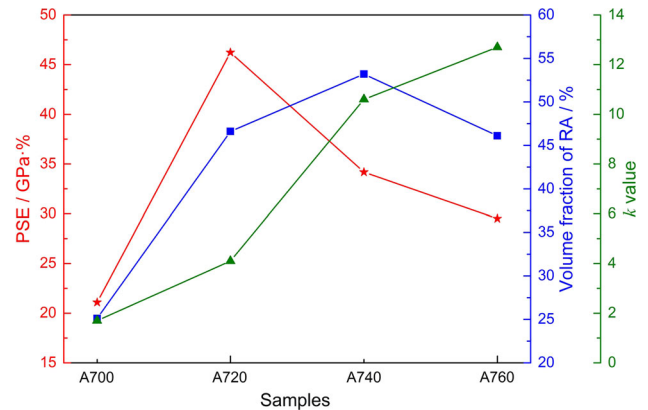


Figure 12 Variation of PSE, volume fraction of RA and k value in A700–A760 steels. k value was calculated by Eq. (3), and a lower k value corresponds to higher mechanical stability of RA.

ratio of austenite to martensite after tensile test of A720 steel were higher than A700 steel (Fig. 5). RA can significantly enhance strength and ductility through TRIP effect [31]. Besides, tensile strength of A740 steel was higher than A720 steel, but total elongation of A740 steel was lower than A720 steel. This is because the mechanical stability of RA in A740 steel was lower than A720 steel (Fig. 12). Although higher content of RA obtained in A740 steel, TRIP effect that occurred in A740 steel during deformation may finish at lower strain than A720 steel (Fig. 10), leading to a lower elongation present in A740 steel. Thus, it can be inferred that highest PSE obtained in A720 steel was achieved by a high volume fraction of RA with relatively high mechanical stability. Besides, in A760 steel, RA content and mechanical stability of RA were lower than A740 steel (Fig. 12), such that a lower total elongation was obtained in A760 steel.

Table 3 shows the comparison between medium-Mn steels reported in the literature and experimental steel. A comparatively higher PSE of 46.22 GPa% was obtained in our experimental steel. In contrast, other medium-Mn steels containing high content of Mn had near similar or lower tensile strength with a lower total elongation. Moreover, it should be noted that there was only 4 wt% Mn present in our experimental steel, which can reduce cost and is beneficial to industrial production. Thus, compared to other medium-Mn steels containing high content of Mn reported in the literature, our experimental steel had significantly superior mechanical properties.

Table 3 Comparison between medium-Mn steels reported in the literature and experimental steel

Composition/wt%	Tensile strength/MPa	Total elongation/%	PSE/GPa%	References
Fe–0.13C–6Mn–0.5Si–3.1Al	854	21.7	18.5	[11]
Fe–0.2C–8Mn–4Al	980	33	32.3	[32]
Fe–0.14C–5Mn	910	44.5	40.5	[33]
Fe–0.1C–7.1Mn	876	42	36.8	[17]
Fe–0.18C–6.4Mn–2.8Al–0.5Si	954	39.2	37.4	[34]
Fe–0.25C–4Mn–1.88Al–0.6Si	951	48.6	46.22	Present work

Conclusions

Microstructure, mechanical properties and austenite stability in a novel hot-rolled 4% Mn steel processed by intercritical annealing were studied. The major conclusions are as follows:

1. Thermal stability of intercritical austenite decreased with increase in intercritical annealing temperature, leading to martensite transformation in 740–760 °C intercritically annealed steels. RA content first increased when the intercritical annealing temperature was increased from 700 to 740 °C, followed by a decrease on increasing the intercritical annealing temperature to 760 °C.
2. The 720 °C intercritically annealed steel exhibited excellent combination of yield strength of 766 MPa, tensile strength of 951 MPa, total elongation of 48.6% and PSE of 46.22 GPa%, which were comparable to previously studied medium-Mn steels with high content of Mn.
3. Mechanical stability of RA was significantly influenced by intercritical annealing temperature. Highest PSE obtained in 720 °C intercritically annealed steel was related to the high volume fraction of RA (46.6%) with relatively high mechanical stability. Besides, heterogeneity in grain size, morphology and Schmid factor of RA contributed to the inhomogeneous mechanical stability of RA in 720 °C intercritically annealed steel.

Acknowledgements

The authors acknowledge support from the National Natural Science Foundation of China (No. 51504063) and the Fundamental Research Funds for the Central Universities (N170706002, N160706001). R. D.

K. Misra also gratefully acknowledges continued collaboration with the Northeastern University as honorary professor providing guidance to students in research.

Compliance with ethical standards

Conflict of interest The authors declare that they have no conflict of interest.

References

- [1] Zhao ZZ, Liang JH, Zhao AM, Liang JT, Tang D, Gao YP (2017) Effects of the austenitizing temperature on the mechanical properties of cold-rolled medium-Mn steel system. *J Alloy Compd* 691:51–59
- [2] Lee S, Lee S-J, De Cooman BC (2011) Austenite stability of ultrafine-grained transformation-induced plasticity steel with Mn partitioning. *Scr Mater* 65:225–228
- [3] Yang F, Luo H, Hu C, Pu E, Dong H (2017) Effects of intercritical annealing process on microstructures and tensile properties of cold-rolled 7Mn steel. *Mater Sci Eng, A* 685:115–122
- [4] Hu B, Luo H (2017) A strong and ductile 7Mn steel manufactured by warm rolling and exhibiting both transformation and twinning induced plasticity. *J Alloy Compd* 725:684–693
- [5] Han Y, Shi J, Xu L, Cao WQ, Dong H (2011) TiC precipitation induced effect on microstructure and mechanical properties in low carbon medium manganese steel. *Mater Sci Eng A* 530:643–651
- [6] Park H-S, Seol J-B, Lim N-S, Kim S-I, Park C-G (2015) Study of the decomposition behavior of retained austenite and the partitioning of alloying elements during tempering in CMnSiAl TRIP steels. *Mater Des* 82:173–180
- [7] Lee D, Kim JK, Lee S, Lee K, De Cooman BC (2017) Microstructures and mechanical properties of Ti and Mo micro-alloyed medium Mn steel. *Mater Sci Eng, A* 706:1–14

- [8] Steineder K, Krizan D, Schneider R, Beal C, Sommitsch C (2017) On the microstructural characteristics influencing the yielding behavior of ultra-fine grained medium-Mn steels. *Acta Mater* 139:39–50
- [9] Luo H, Shi J, Wang C, Cao W, Sun X, Dong H (2011) Experimental and numerical analysis on formation of stable austenite during the intercritical annealing of 5Mn steel. *Acta Mater* 59:4002–4014
- [10] Shi J, Sun X, Wang M, Hui W, Dong H, Cao W (2010) Enhanced work-hardening behavior and mechanical properties in ultrafine-grained steels with large-fractioned metastable austenite. *Scr Mater* 63:815–818
- [11] Suh DW, Park SJ, Lee TH, Oh CS, Kim SJ (2010) Influence of Al on the microstructural evolution and mechanical behavior of low-carbon, manganese transformation-induced-plasticity steel. *Metall Mater Trans A* 41:397–408
- [12] Li ZC, Ding H, Misra RDK, Cai ZH, Li HX (2016) Microstructural evolution and deformation behavior in the Fe-(6, 8.5) Mn–3Al–0.2 C TRIP steels. *Mater Sci Eng, A* 672:161–169
- [13] Cai ZH, Ding H, Misra RDK, Ying ZY (2015) Austenite stability and deformation behavior in a cold-rolled transformation-induced plasticity steel with medium manganese content. *Acta Mater* 84:229–236
- [14] Hong H, Lee OY, Song KH (2003) Effect of Mn addition on the microstructural changes and mechanical properties of C-Mn TRIP Steels. *J Korean Soc Heat Treat* 16:205–210
- [15] Hu B, Luo H, Yang F, Dong H (2017) Recent progress in medium-Mn steels made with new designing strategies, a review. *J Mater Sci Technol* 33:1457–1464
- [16] Gibbs PJ, De Moor E, Merwin MJ, Clausen B, Speer JG, Matlock DK (2011) Austenite stability effects on tensile behavior of manganese-enriched-austenite transformation-induced plasticity steel. *Metall Mater Trans A* 42:3691–3702
- [17] Sun B, Fazeli F, Scott C, Yue S (2016) Phase transformation behavior of medium manganese steels with 3 wt pct aluminum and 3 wt pct silicon during intercritical annealing. *Metall Mater Trans A* 47:4869–4882
- [18] Seo EJ, Cho L, Estrin Y, De Cooman BC (2016) Microstructure-mechanical properties relationships for quenching and partitioning (Q&P) processed steel. *Acta Mater* 113:124–139
- [19] Sugimoto KI, Usui N, Kobayashi M, Hashimoto SI (1992) Effects of volume fraction and stability of retained austenite on ductility of TRIP-aided dual-phase steels. *ISIJ Inter* 32:1311–1318
- [20] Timokhina IB, Hodgson PD, Pereloma EV (2007) Transmission electron microscopy characterization of the bake-hardening behavior of transformation-induced plasticity and dual-phase steels. *Metall Mater Trans A* 38:2442–2454
- [21] Wang J, van der Zwaag S (2001) Stabilization mechanisms of retained austenite in transformation-induced plasticity steel. *Metall Mater Trans A* 32:1527–1539
- [22] De Moor E, Matlock DK, Speer JG, Merwin MJ (2011) Austenite stabilization through manganese enrichment. *Scr Mater* 64:185–188
- [23] Jimenez-Melero E, van Dijk NH, Zhao L, Sietsma J, Offerman SE, Wright JP, van der Zwaag S (2007) Martensitic transformation of individual grains in low-alloyed TRIP steels. *Scr Mater* 56:421–424
- [24] Sohn SS, Lee BJ, Lee S, Kim NJ, Kwak JH (2013) Effect of annealing temperature on microstructural modification and tensile properties in 0.35 C–3.5 Mn–5.8 Al lightweight steel. *Acta Mater* 61:5050–5066
- [25] Sugimoto K, Kobayashi M, Hashimoto S (1992) Ductility and strain-induced transformation in a high-strength transformation-induced plasticity-aided dual-phase steel. *Metall Mater Trans A* 23:3085–3095
- [26] Xu YB, Zou Y, Hu ZP, Han DT, Chen SQ, Misra RDK (2017) Correlation between deformation behavior and austenite characteristics in a Mn-Al type TRIP steel. *Mater Sci Eng A* 698:126–135
- [27] Cai ZH, Ding H, Misra RDK, Kong H (2014) Unique serrated flow dependence of critical stress in a hot-rolled Fe–Mn–Al–C steel. *Scr Mater* 71:5–8
- [28] Cai ZH, Ding H, Xue X, Xin QB (2013) Microstructural evolution and mechanical properties of hot-rolled 11% manganese TRIP steel. *Mater Sci Eng A* 560:388–395
- [29] Ding R, Tang D, Zhao A, Guo H, He J, Zhi C (2015) Effect of ultragrain refinement on quenching and partitioning steels manufactured by a novel method. *Mater Des* 87:640–649
- [30] Seo CH, Kwon KH, Choi K, Kim KH, Kwak JH, Lee S, Kim NJ (2012) Deformation behavior of ferrite–austenite duplex lightweight Fe–Mn–Al–C steel. *Scr Mater* 66:519–522
- [31] Wang HS, Kang J, Dou WX, Zhang YX, Yuan G, Cao GM, Misra RDK, Wang GD (2017) Microstructure and mechanical properties of hot-rolled and heat-treated TRIP steel with direct quenching process. *Mater Sci Eng A* 702:350–359
- [32] Cai Z, Ding H, Ying Z, Misra RDK (2014) Microstructural evolution and deformation behavior of a hot-rolled and heat treated Fe-8Mn-4Al-0.2 C steel. *J Mater Eng Perform* 23:1131–1137
- [33] Sun R, Xu W, Wang C, Shi J, Dong H, Cao W (2012) Work hardening behavior of ultrafine grained duplex medium-Mn steels processed by ART-annealing. *Steel Res Int* 83:316–321
- [34] Xu YB, Hu ZP, Zou Y, Tan XD, Han DT, Chen SQ, Ma DG, Misra RDK (2017) Effect of two-step intercritical annealing on microstructure and mechanical properties of hot-rolled medium manganese TRIP steel containing δ -ferrite. *Mater Sci Eng A* 688:40–55